PAPER • OPEN ACCESS

Mask-based dual-axes tomoholography using soft x-rays

New Journal of Physics
The open access journal at the forefront of physics

Deutsche Physikalische Gesellschaft DPG
IOP Institute of Physics

Published in partnership with: Deutsche Physikalische Gesellschaft and the Institute of Physics

OPEN ACCESS

RECEIVED
24 July 2015

REVISED
21 September 2015

ACCEPTED FOR PUBLICATION
29 September 2015

PUBLISHED
21 October 2015

PAPER

Mask-based dual-axes tomoholography using soft x-rays

Erik Guehrs[1], Manuel Fohler[2], Stefanie Frömmel[1], Christian M Günther[1], Piet Hessing[1], Michael Schneider[1], Laura Shemilt[1] and Stefan Eisebitt[1,2]

[1] Institut für Optik und Atomare Physik, Technische Universität Berlin, Hardenbergstr. 36, D-10623 Berlin, Germany
[2] Helmholtz-Zentrum Berlin für Materialien und Energie, Albert-Einstein-Straße 15, D-12489 Berlin, Germany

E-mail: erik.guehrs@tu-berlin.de

Keywords: tomography, x-ray FTH, HERALDO

Supplementary material for this article is available online

Abstract

We explore tomographic mask-based Fourier transform x-ray holography with respect to the use of a thin slit as a reference wave source. This imaging technique exclusively uses the interference between the waves scattered by the object and the slit simplifying the experimental realization and ensuring high data quality. Furthermore, we introduce a second reference slit to rotate the sample around a second axis and to record a dual-axes tomogram. Compared to a single-axis tomogram, the reconstruction artifacts are decreased in accordance with the reduced missing data wedge. Two demonstration experiments are performed where test structures are imaged with a lateral resolution below 100 nm.

1. Introduction

Fourier transform holography (FTH) with x-rays is a high-resolution imaging technique based on coherent scattering. In FTH, the interference pattern of a reference wave and the scattering from the object is detected in the far-field region [1, 2]. The reference wave is generated by a reference structure located in the sample plane. Due to the holographic encoding of amplitude and phase, an image of the object can be extracted by direct Fourier inversion. In addition, the wavefield generated by the object can be inspected in different planes along the optical axis through back propagation [3, 4]. Virtual optics can be employed to calculate the effect of different optical transformations of the wavefront, obtaining e.g. Zernike phase contrast [5].

Soft x-ray FTH is usually performed using a mask based approach [2, 6, 7], i.e. object and reference beams originate from apertures in the object plane. The mask-based experimental scheme is very robust as virtually all transmitted light contains information on either the object or the reference. Furthermore, if the mask and the object to be imaged are monolithically connected to each other, sample drift during exposure does not affect the imaging process.

A typical mask is made of a high-Z element material, with a thickness of 1μm. For high resolution a conically tapering circular reference hole with a diameter below 100 nm is used, thus yielding an aspect ratio of 1:5. Consequently, the transmission through the circular reference aperture is already blocked at tilt angles of approximately $\arctan(0.2) \approx 11°$, resulting in an accessible angular range which is too small for tomography.

Nevertheless, it is possible to combine soft-x-ray FTH with tomography using an optically inverted sample design: the reference aperture is replaced by a small absorber or scatterer, located on a transparent support membrane in close proximity to the object to be imaged [8]. While this open-membrane approach allows for sample rotation and retains the advantages of monolithically coupling the sources of object and reference waves, the large amount of directly transmitted light creates a large background intensity in the hologram. As it is in practice difficult to entirely block this radiation using a central beam block, this approach requires a much better experimental control over the x-ray illumination and the signal-to-noise ratio achieved with this method is typically reduced compared to FTH using an opaque mask.

Here, we demonstrate an approach using an opaque mask in conjunction with tomographic x-ray holography ('tomoholography') to obtain a 3D image of the sample. We use a slit-shaped aperture to produce

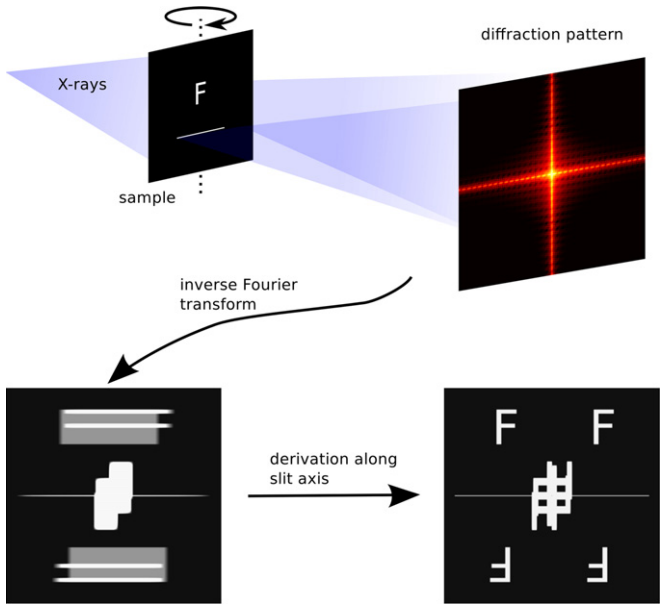

Figure 1. If a thin slit is used as reference wave source the inverse Fourier transform of the hologram results in a crosscorrelation between slit and object. The real space image of the object can be reconstructed by derivation along the slit-axis, according to the HERALDO approach [9–11]. Rotation around the axis indicated is possible, as long as the projected length of the reference line is sufficient to separate the reconstructed images.

the reference wave. This is a special case of 'holography with extended reference by linear autocorrelation' (HERALDO, compare figure 1) where extended reference structures in conjunction with a numerical operation such as differentiation are used for holographic imaging [9–11]. Obviously, such a mask can be rotated perpendicular to the reference slit axis over a large angular range while still retaining the capability to generate a reference wave at the endpoints of the slit where the transmission ends abruptly [12].

For a full tomographic dataset a 180° rotation of the sample is necessary. A restricted angular range leads to a missing wedge in the data with an associated loss in information and associated imaging artifacts [13]. For the opaque mask approach explored here, the angular range is always restricted to $<180°$ due to geometric reasons. To decrease the missing information, we introduce a second reference slit orthogonal to the first one. In this way it is possible to record an orthogonal tilt series from the same sample. Consequently, the missing wedge is reduced to a missing pyramid and the quality of the 3D reconstruction can be improved [13, 14].

2. Methods

To demonstrate this concept we prepared two test samples, shown in figure 2. The first sample consists of a lithographic structure depicting the 'Brandenburg Gate' in Berlin. To prepare the sample, a circular object aperture and two orthogonal, narrow reference apertures were created by focused ion beam (FIB) milling in a 1μm thick gold film. Previously, the gold film was deposited on the silicon nitride membrane (1×1 μm^2 thickness 100 nm) by thermal evaporation. The Brandenburg Gate was fabricated by FIB assisted platinum deposition. It has lateral dimensions of approximately 1.3 μm $\times$ 1.25 μm and a platinum thickness of approximately 0.5μm.

As a second sample we used the shell of a diatom. For the preparation, a droplet from an aqueous suspension of diatoms was deposited on a silicon nitride membrane, which had been coated with a gold film of 1μm thickness on the opposite side. After the solvent evaporated a circular object hole was generated at a suitable position, selecting a single diatom. The required coordinate transfer between the front and back side of the sample was achieved by FIB milling through holes as markers, which were later on covered by FIB-assisted Pt deposition, as seen in figure 2. Again, two orthogonal reference apertures were created. Typical circular references were produced in the holographic mask of both samples to provide a comparison to the HERALDO reconstruction. Both samples are surrounded by platinum dots used as fiducial markers for alignment of the different 2D projections. These platinum dots have a diameter of 80 nm for the Brandenburg Gate and of 150 nm for the diatom sample.

Tomographic series of holograms of the Brandenburg gate test sample were recorded at the BESSY II undulator beamline U41-PGM at a photon energy of 600 eV, while the diatom sample was measured at the

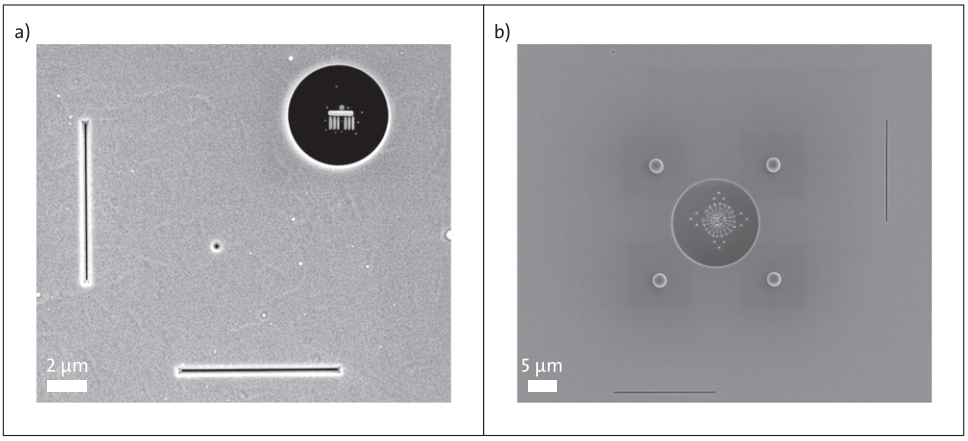

Figure 2. Scanning electron micrographs of the samples. (a) A test object with the shape of a 'Brandenburg Gate' consisting out of deposited platinum and (b) a single shell of a diatom are located in the middle of the respective object hole. In both cases two thin slits are used as reference wave source milled through the x-ray opaque gold film. The slits allow for rotation around two perpendicular axes such that the reference wave from one of the slits is usable for hologram generation over a large angular range. As a result, a dual-axes data set can be measured. For comparison with standard FTH, both samples contains a small reference hole. The four large dot structures in (b) are part of the test sample fabrication process and are inconsequential in the holographic image formation process.

UE52-SGM beamline using a photon energy of 200 eV. Samples were mounted on a $xyz\varphi$-manipulator which allowed for rotation of the sample in the vacuum chamber. The rotation axis, which was perpendicular to the respective reference slit used, was aligned to intersect the test object, thus simplifying data analysis and image reconstruction.

Holograms are recorded on an in-vacuum, back-illuminated charge-coupled device (CCD) camera (2048×2048 pixels, pixel size 13.5 μm) 32 cm behind the samples, allowing for sufficiently high sampling frequency. The central part of the hologram is blocked by a beam stop to use the limited dynamic range of the CCD to preferentially record high spatial frequency information of the samples.

3. Results and discussion

In total 30 holograms of the Brandenburg Gate test sample are recorded for both rotational axes from $\varphi = -60°$ to $+56°$ in $4°$ steps. The maximum tilt angles are limited by the aspect ratio of membrane width and the thickness of the surrounding silicon frame. The total exposure time is adapted for each hologram (14 s to 60 s) to ensure that sufficient signal is collected to sample hologram fringes up to the edge of the CCD, corresponding to a momentum transfer of $q = 131\ \mu\text{m}^{-1}$.

For the diatom sample 39 holograms are recorded from $\varphi = -57°$ to $+57°$ in $3°$ steps for both rotational axes. Here, the maximum momentum transfer recorded on the CCD is $q = 44\ \mu\text{m}^{-1}$ and the illumination time for each hologram is 30 s to 100 s.

Holograms and image reconstructions of both samples are shown in figure 3. For each angular position a real-space image of the objects can be retrieved using the HERALDO concept. As expected, the quality of the HERALDO image reconstruction is very similar to the standard FTH image reconstruction, employing a pinhole reference. Both reconstructions are not superimposed by stray light artifacts as virtually only light scattered by the object and the references are recorded on the CCD. Note, that the transmission through the pinhole is blocked at angular positions larger than $\pm 12°$, as expected.

The lateral resolution of the HERALDO reconstruction for the Brandenburg Gate at $0°$ is 60 nm as determined from the power spectrum averaging over all spatial directions. The lateral resolution along the direction of the slit can in principle change as a function of the angular position [15]. The gradient of the x-ray transmission at the end of the slit may change with rotation and hence can influence the lateral resolution of the projections along the slit direction. In our experiment, we find the lateral resolution along the horizontal axis (along the slit axis) to vary between 60 nm and 150 nm due to this effect. The vertical resolution (perpendicular to the slit axis) is not affected by rotation and is $\approx$60 nm for all angular positions. Note, that the horizontal and vertical resolution are determined using the 90%–10% knife-edge criterion (data not shown).

The lateral resolution for the diatom at $0°$ to the incident x-ray beam is 100 nm and varies between 90 nm and 180 nm for the different rotational positions of the sample. It is better than the lateral resolution obtained for the Brandenburg Gate test sample because (i) the maximum momentum transfer accepted by the CCD is

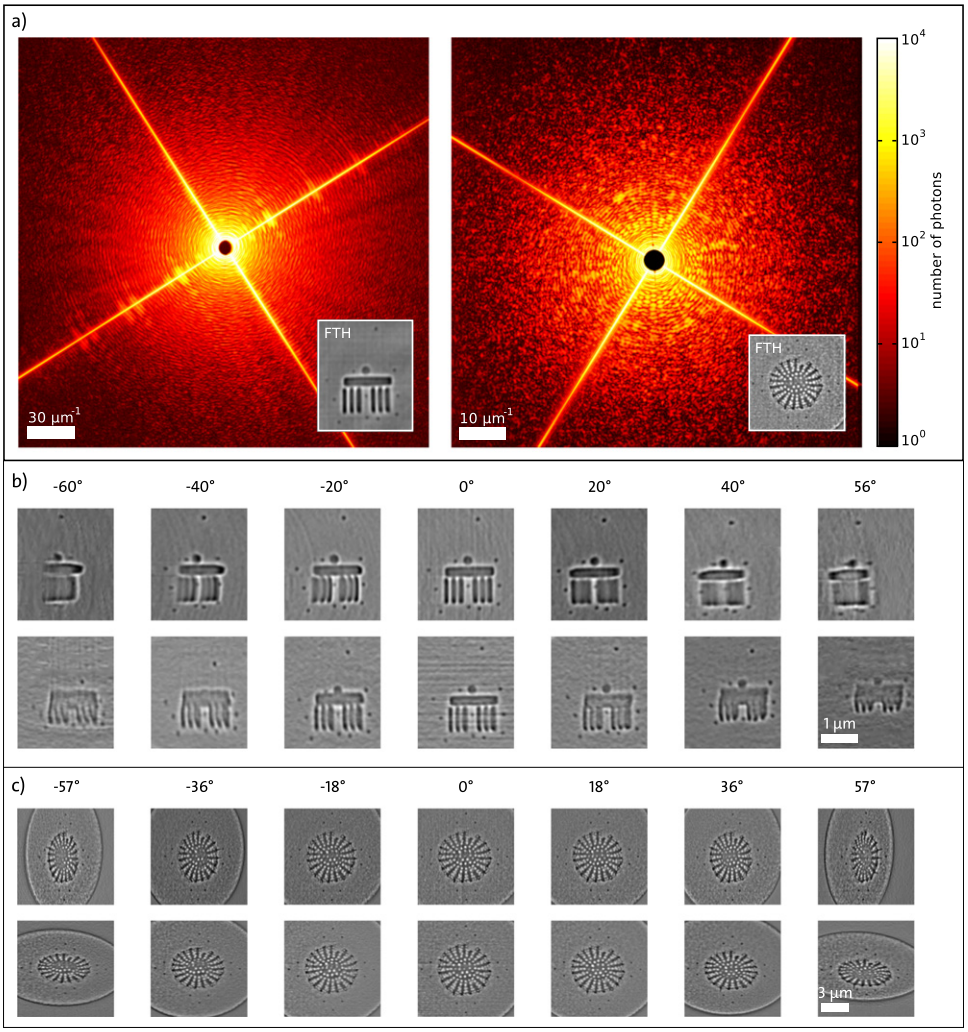

Figure 3. (a) Holograms of the Brandenburg Gate test object (left) and the diatom (right) at normal incidence (0°) of the x-ray beam. For comparison with HERALDO the inset in both holograms shows the standard, single pinhole FTH reconstruction at normal incidence light. For all angular positions of both samples a 2D projection image can be reconstructed by HERALDO. As examples, some of the 2D image reconstructions of the Brandenburg Gate (b) and the diatom (c) are shown. On the top row within panel (b) and (c), 2D reconstructions are presented where the sample is rotated around the vertical axis while the bottom rows show rotation around the horizontal axis.

smaller due to the longer x-ray wavelength and (ii) the width of the slit is larger, reducing the spatial resolution primarily in the direction perpendicular to the slit to ≈60 nm for the Brandenburg Gate and ≈140 nm for the diatom sample.

For both samples, the tomographic image reconstruction is computed using the IMOD software package [16]. The small markers surrounding the specimens are used as fiducial markers to determine the exact angular position and the axis of rotation for each projection. The aligned 2D images are used to calculate the tomogram by a weighted filtered back-projection. The voxel size of the resulting tomograms is 12 × 12 × 12 nm^3 for the Brandenburg Gate and 36 × 36 × 36 nm^3 for the diatom, respectively.

In figure 4 slices through the tomogram of the Brandenburg Gate test sample are shown. The six 'vertical' pillars of the Brandenburg Gate as well as the 'horizontal' beam ('architrave') above are clearly visible in the reconstruction. Some of the pillars are tilted up to 14° away from the substrate normal, which is in agreement with the electron microscopy information. The height of the pillars and the top is determined to be 500 nm and 700 nm, respectively.

The tomogram of the diatom is shown in figure 5. It can be seen that the diatom is not a flat structure. The inner part of the shell slightly bulges out of the plane. At its fringe, the diatom features some spikes in the reconstruction, and it is possible to distinguish between longer spikes approximately 700 nm in length, and shorter, presumably broken spikes of approximately 450 nm in length. Based on the tomograms, surface models of both samples are calculated (shown in figures 4(c) and 5(c)). Movies of different views of the 3D models and of the slices through the tomograms are available online as supplementary information. The quality of the 3D

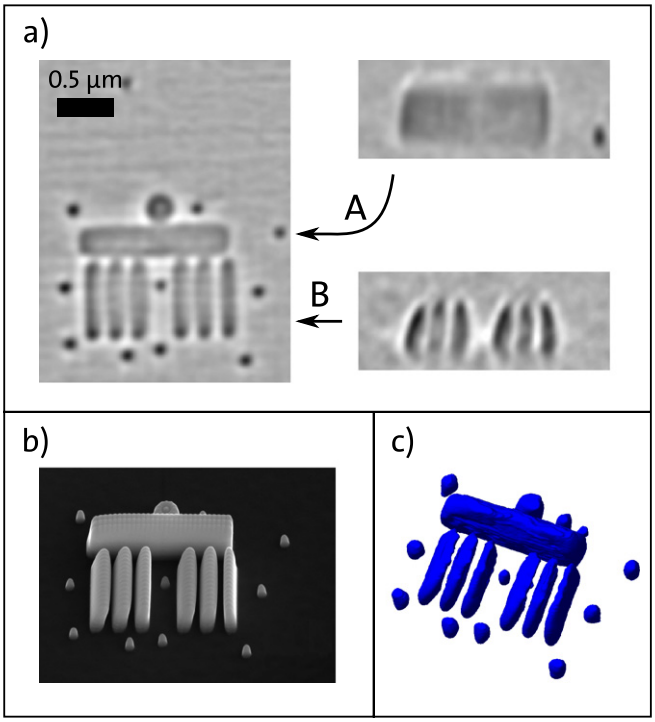

Figure 4. (a) Slices from top (left) and side view (right) through the tomogram of the Brandenburg Gate. The arrows indicate the position of the slices in the side view. On the basis of the tomogram a 3D rendered model of the surface is calculated (c). For comparison, an electron micrograph of the sample is shown in (b). The scale bar in (a) refers to all panels.

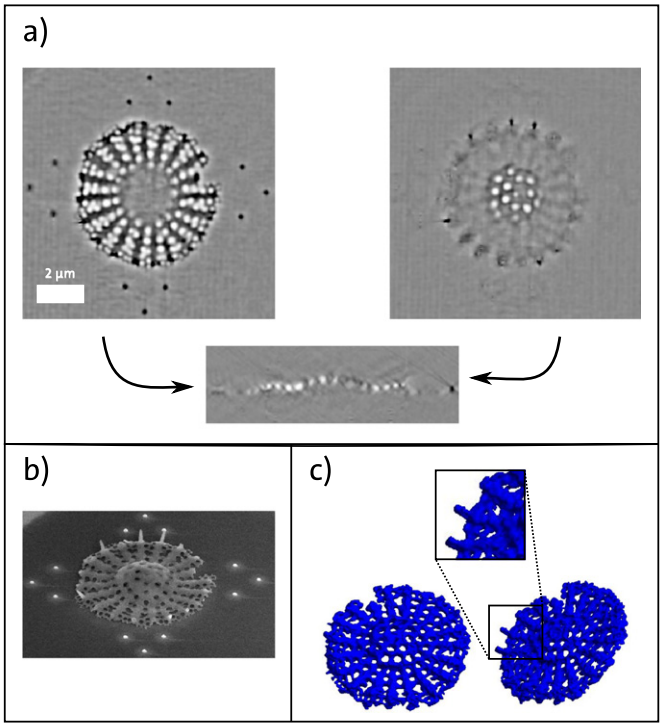

Figure 5. (a) Slices from top (top) and side view (bottom) through the tomogram of the diatom. The arrows indicate the position of the slices in the top view. On the base of the tomogram a 3D rendered model of the shell of the diatom is calculated. Several views of the model are shown in (c) and the some of the longer spikes are highlighted in the inset. For comparison an electron micrograph of the sample is shown in (b). The two micron scale bar refers to all panels of the figure except for the inset in panel (c).

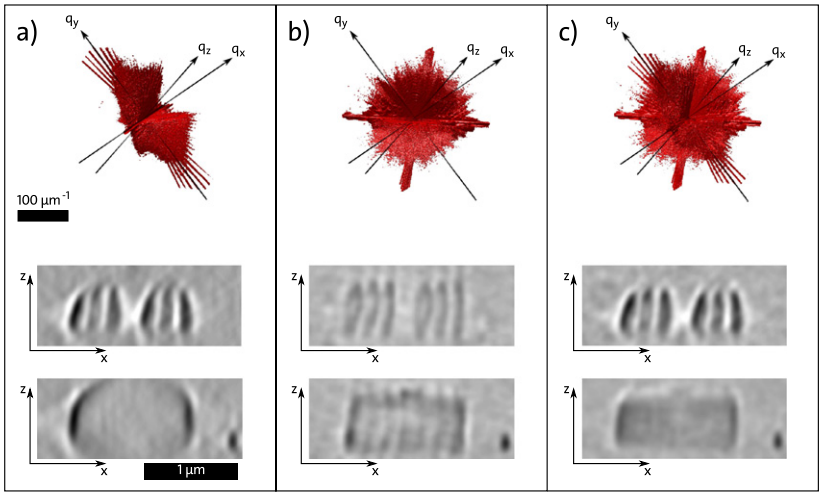

Figure 6. Comparison of single-axis tomoholography with dual-axes tomoholography. The tomographic reconstruction for the rotation around the vertical axis is shown in (a), around the horizontal axis in (b) and for both axes in (c). The middle row shows slices from side views at the position of the six pillars of the Gate while the bottom row displays slices through the architrave at the top of the Gate, corresponding to the arrows B and A in figure 4(a), respectively. At the top the respective holograms used for reconstruction are plotted as 3D representations. The missing information is visible as a missing wedge in (a) and (b). In (c) the missing information is reduced to a missing pyramid. The observed tomographic reconstruction artifacts of the single-axis tomograms can be explained by the position of the corresponding missing wedges. By combining both data sets to a dual-axes tomogram these artifacts can be reduced (see text for more details).

image reconstruction is very similar to the reconstruction of the diatom obtained in a previous result where a gold sphere was used as reference wave source [8]. The benefit of this work is the introduction of a second tilt axis which is very important for 3D imaging of anisotropic objects.

To illustrate the effect of recording a second tilt series, we also reconstructed tomograms from each single tilt axis of the Brandenburg Gate test sample. In figure 6(a) the tomogram of the Brandenburg Gate, as rotated around the vertical axis, is shown. Here, strong artifacts can be seen at the horizontal top. In contrast, the six pillars are reconstructed with a similar quality to the dual-axes tomogram. The opposite occurs for the rotation around the horizontal axis (compare figure 6(b)), where the pillars show stronger artifacts.

These reconstruction artifacts are caused by the limited angular range leading to missing information. In microscopy based tomography this is known as missing wedge [13, 14]. These information gaps are illustrated in the top row of panels in figure 6. For each axis of rotation, all holograms used in the reconstruction, are arranged to a 3D diffraction pattern. It can be seen that the missing wedge of the horizontal and vertical tilt series are located perpendicular to each other (shown in figures 6(a) and (b)). The resulting different artifacts within each tomogram depend on which part of the sample's 3D spatial frequency spectrum is sampled. For example in figure 6, information on linear edge structures scattering into missing data volumes is lost. This effect is clearly visible at the edge of the architrave along the *x*-axis which is not visible at all in (a) and the *y*-axis in (b), where the clear 'height' separation between the architrave and the pillars is lost.

The simple mask-design used here allows to introduce a second slit to record a second tilt series of the same sample. As long as the holographic separation conditions are fulfilled the image reconstructions of the different references do not influence each other. The fact that the object and all reference structures are monolithically locked relatively to each other in the same mask allows for easy combination of the tomography data obtained for rotation around the different axes. By combining both HERALDO datasets to a dual-axes tomogram, reconstruction artifacts are strongly reduced as the missing information is reduced from a wedge to a missing pyramid. For example in figure 6(c), the architrave now has clear boundaries both in the *xz*-plane as well as along the *y*-axis. Compared to a single-axis tomogram the amount of missing data is decreased and thus less structural information of the sample is lost.

4. Summary

We demonstrated a simple and robust dual-axes tomoholography concept, based on HERALDO. In our mask-based approach, data from different (e.g. orthogonal) rotation axes can easily be combined. As virtually only x-rays scattered by the object and the reference structures can reach the detector, the experimental difficulties

related to limited dynamic range of the detector and directly transmitted radiation as well as pertaining to 'clean' (i.e. locally defined) illumination of the sample are greatly reduced.

As proof of principle, we reconstructed tomograms of two test objects. In both cases, we obtain diffraction limited resolution and we can reduce the missing wedge artifacts by the introduction of the second rotation axis. As a result the tomograms have a higher quality than tomograms recorded with a single axis of rotation. In contrast to obtaining 3D information via a single, high numerical aperture hologram [4] this tomographic approach allows for an isotropic spatial resolution in 3D—with the exception of sample spatial frequencies falling into the missing data pyramid.

Recently, it was demonstrated that the depth information could be extracted from a single x-ray hologram using the opaque mask-design. This was achieved by the propagation of the reconstructed complex wave-field through different planes of the sample [4]. In contrast to tomography, the lateral and longitudinal resolution differ from each other by an order of magnitude and the objects to be imaged must be separated laterally from each other. However, a great advantage of this method is that 3D information can be extracted from a single view.

In principle our approach can be used to image a large variety of objects in 3D as long as they can be positioned on the object aperture of an opaque gold mask. In particular, we note that our approach may be useful in determining vector quantities such as e.g. 3D magnetic moments in a 2D sample, extending on the work by Duckworth *et al* [12].

Acknowledgments

We thank Peter Guttman from the Helmholtz-Zentrum Berlin for providing the diatoms.

References

[1] McNulty I, Kirz J, Jacobsen C, Anderson E H, Howells M R and Kern D P 1992 High-resolution imaging by fourier transform x-ray holography *Science* **256** 1009–12
[2] Eisebitt S, Lörgen M, Eberhardt W, Lüning J, Andrews S and Stöhr J 2004 Scalable approach for lensless imaging at x-ray wavelengths *Appl. Phys. Lett.* **84** 3373–5
[3] Guehrs E, Günther C M, Pfau B, Rander T, Schaffert S, Schlotter W F and Eisebitt S 2010 Wavefield back-propagation in high-resolution x-ray holography with a movable field of view *Opt. Express* **18** 18922–31
[4] Geilhufe J, Tieg C, Pfau B and Günther C M 2014 Extracting depth information of 3-dimensional structures from a single-view x-ray Fourier-transform hologram *Opt. Express* **22** 24959–69
[5] Guehrs E, Günther C M, Könnecke R, Pfau B and Eisebitt S 2009 Holographic soft x-ray omni-microscopy of biological specimens *Opt. Express* **17** 6710–20
[6] Günther C M *et al* 2010 Microscopic reversal behavior of magnetically capped nanospheres *Phys. Rev. B: Condens. Matter* **81** 64411
[7] Pfau B *et al* 2011 Origin of magnetic switching field distribution in bit patterned media based on pre-patterned substrates *Appl. Phys. Lett.* **99** 062502
[8] Guehrs E, Stadler A M, Flewett S, Frömmel S, Geilhufe J, Pfau B, Rander T, Schaffert S, Büldt G and Eisebitt S 2012 Soft x-ray tomoholography *New J. Phys.* **14** 013022
[9] Guizar-Sicairos M and Fienup J R 2007 Holography with extended reference by autocorrelation linear differential operation *Opt. Express* **15** 17592–612
[10] Guizar-Sicairos M and Fienup J R 2008 Direct image reconstruction from a Fourier intensity pattern using HERALDO *Opt. Lett.* **33** 2668–70
[11] Guizar-Sicairos M, Zhu D, Fienup J R, Wu B, Scherz A and Stöhr J 2010 Holographic x-ray image reconstruction through the application of differential and integral operators *Opt. Lett.* **35** 928–30
[12] Duckworth T *et al* 2013 Holographic imaging of interlayer coupling in Co/Pt/NiFe *New J. Phys.* **15** 023045
[13] Penczek P A and Frank J 2006 Resolution in electron tomography *Electron Tomography: Methods for Three-Dimensional Visualization of Structures in the Cell* 2nd edn ed J Frank (New York: Springer) ch 10, pp 307–330
[14] Radermacher M 2006 Weighted back-projected methods *Electron Tomography: Methods for Three-Dimensional Visualization of Structures in the Cell* 2nd edn ed J Frank (New York: Springer) ch 8, pp 245–273
[15] Könnecke R 2010 Multiple and extended references in Fourier transform holography *PhD Thesis* Technische Universität Berlin
[16] Kremer J R, Mastronarde D N and McIntosh J R 1996 Computer visualization of three-dimensional image data using IMOD *J. Struct. Biol.* **116** 71–6